Fiber Bundle Models for Composite Materials

F. Raischel, F. Kun and H.J. Herrmann

Abstract

In this paper we will outline the advantages of using fiber bundles in modeling disordered materials. We will present the main aspects of classical fiber bundle models (FBMs) and highlight their ability to capture some essential aspects of composite materials. We then present some extensions of the classical FBM, modifying the way of interaction of fibers, failure law, deformation state and constitutive behavior. The subclasses of FBMs which we generate in this way, i.e., the variable range of interaction model, the continuous damage FBM, the beam model, and the plastic FBM, will turn out to overcome some of the limitations of classical FBMs. We will discuss the characteristic dynamics of these model systems and give references to experiments.

1 Introduction

From the viewpoint of statistical physics, unidirectional fibrous composites can be reduced to just a few characteristic properties: firstly, they contain load-carrying fibers embedded in a matrix material which carries a negligible amount of load, but provides for the load transfer between broken and unbroken fibers. Secondly, the material is highly anisotropic, so a characteristic picture can be obtained by considering an uniaxial loading condition, with the load being applied in the fibers' direction. Thirdly, the load bearing capacity of the fibers is highly disordered, necessitating a description in terms of *disordered materials*. Finally, a complete dynamical description of the failure process needs to account for the load distribution processes that occur when a fiber ruptures and its load has to be carried by the remaining intact fibers. Fiber bundle models (FBMs) —as we will show in the following— naturally provide these characteristics, and recent developments and additions have made them more applicable to a broad variety of experimental situations.

The damage and fracture of disordered materials is a very important scientific and technological problem which has attracted intensive research over the past decades. One of the first theoretical approaches to the problem was the fiber bundle model introduced by Peires in 1927 to understand the strength of cotton yarns [1]. In his pioneering work, Daniels provided the probabilistic formulation of the model and carried out a comprehensive study of bundles of threads assuming equal load sharing after subsequent failures [2]. In order to capture fatigue and creep effects, Coleman proposed a time dependent formulation of the model [3], assuming that the strength of loaded fibers is a decreasing function of time. Later on these early works initiated an intense research in both the engineering [4] and physics [5; 6; 7] communities making fiber bundle models one of the most important theoretical approaches to the damage and fracture of disordered materials [8]. Whereas from the engineering point of view, FBMs are a starting point to develop more realistic micromechanical models of the failure of fiber reinforced composites, physicists are primarily concerned with embedding the failure and breakdown of materials into the general framework of statistical physics and clarifying its analogy to phase transitions and critical phenomena.

In this article we first present the basic formulation of the classical fiber bundle model. We then discuss limitations of the model to describe the fracture of fiber reinforced composites and propose extensions which make the model more realistic.

2 The Classical Fiber Bundle Model

The disordered solid is represented as a discrete set of parallel fibers of number N, organized on a regular lattice, see Fig. 1a. The fibers can solely support longitudinal deformation which allows to study only loading of the bundle parallel to fibers. When the bundle is subjected to an increasing external load F, the fibers behave linearly elastic until they break at a failure load $\sigma_{th}^i,\ i = 1, \ldots, N$, as it is illustrated in Fig. 1b. The elastic behavior of fibers is characterized by the Young modulus E, which is identical for all fibers. The strengths σ_{th}^i are independent identically distributed random variables with the probability density $p(\sigma_{th})$ and distribution function $P(\sigma_{th})$. The randomness of breaking thresholds is assumed to represent the disorder of heterogeneous materials. A widely used distribution in FBMs is the Weibull distribution

$$P(\sigma_{th}) = 1 - \exp\left[-\left(\frac{\sigma_{th}}{\lambda}\right)^m\right], \qquad (1)$$

where m and λ denote the Weibull index and scale parameter, respectively.

After a fiber has failed, its load has to be shared by the remaining intact fibers. Historically, two extremal cases of

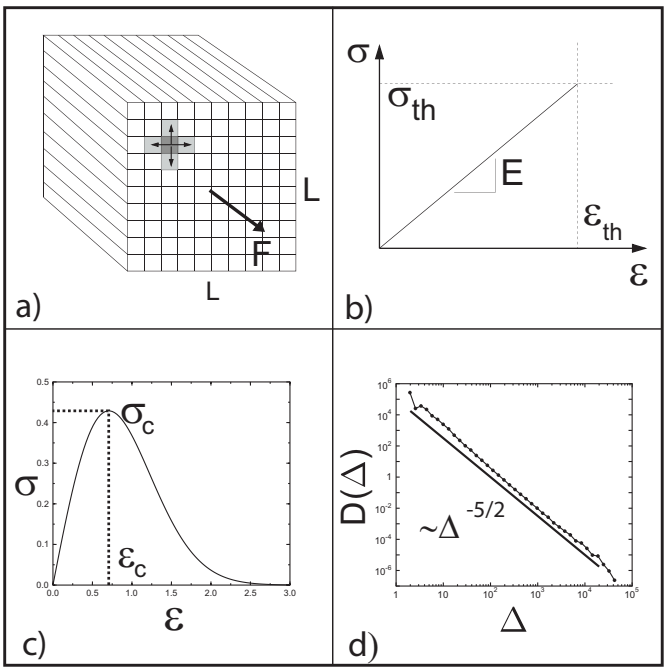

Figure 1: a) Schematic FBM setup. b) Constitutive curve of a single fiber. c) Typical constitutive curve of a fiber bundle. d) Typical avalanche size distribution under GLS.

load sharing are distinguished: in global load sharing (GLS), the load is equally redistributed over all intact fibers in the bundle. In the other case of local load sharing (LLS), the entire load of the failed fiber is redistributed equally over its local neighborhood (usually nearest neighbors) in the lattice considered, leading to stress concentrations along failed regions (see Fig. 1a). Contrary to GLS models, LLS problems normally have to be solved numerically.

Loading of a bundle of fibers can be performed in two ways: when the deformation ε of the bundle is controlled externally, the load on single fibers σ_i is always determined by the externally imposed deformation ε, i.e. no load sharing occurs and consequently the fibers break one-by-one in the increasing order of their breaking thresholds. The macroscopic constitutive behavior of the FBMs then takes the form

$$\sigma(\varepsilon) = E\varepsilon\left[1 - P(E\varepsilon)\right], \tag{2}$$

where $[1 - P(E\varepsilon)]$ is the fraction of intact fibers at the deformation ε [7; 9]. A representative example of $\sigma(\varepsilon)$ is presented in Fig. 1c for the case of Weibull distributed strength values.

With stress controlled conditions, after each fiber breaking the load dropped by the broken fiber has to be redistributed over the surviving intact ones. The subsequent load redistribution after consecutive fiber failures can lead to an entire avalanche of breakings. For GLS, it was found that for a broad class of disorder distributions, the distribution D of avalanches of sizes Δ follows a power law distribution with an exponent $5/2$ [10; 11]

$$D(\Delta) \propto \Delta^{-5/2} \tag{3}$$

see Fig. 1d.

Hence, under stress controlled loading, the constitutive curve Eq. 2 can only be realized up to the maximum at $(\varepsilon_c, \sigma_c)$, where a catastrophic avalanche occurs breaking all the remaining fibers. Increasing the size N of finite bundles, the global strength $\sigma_c(N)$ rapidly converges to the finite non-zero strength of the infinite bundle [2; 4; 9].

If the load sharing is localized, the macroscopic response of the bundle follows the functional form of Eq. 2 but becomes more brittle, i.e. failure occurs at a lower critical stress $\sigma_c^{LLS} < \sigma_c^{GLS}$, which is preceded by only a weak non-linearity [12]. Large scale computer simulations revealed that in the thermodynamic limit $N \to \infty$, the strength of LLS bundles tends to zero as $1/(\ln N)$ [13].

On the micro-level the damage evolution also depends on the type of load sharing: under GLS, no spatial correlations arise, i.e. fiber breaking proceeds in a completely stochastic manner in space which results in randomly nucleated clusters of broken fibers analogous to percolation. Under LLS, however, load localization leads to a formation of clusters of broken fibers. It should be noted that from an experimental point of view, avalanches of breaking fibers correspond to acoustic emission signals, and the cluster structure of failed fibers can —at least in principle— be recorded by imaging techniques.

3 Variable Range of Interaction

In this section we introduce a one-parameter load transfer function to obtain a more realistic description of the interaction of fibers [12]. Varying its parameter, the load transfer function interpolates between the two limiting cases of load redistribution, i.e. the GLS and LLS schemes.

3.1 Load transfer function

The fracture of heterogeneous systems is characterized by the highly localized concentration of stresses at the crack tips that induces the nucleation of new micro-cracks in these regions, leading to the growth of the crack and to the final failure of the system. In elastic materials, the stress distribution around cracks follows a power law

$$\sigma_{add} \sim r^{-\gamma}, \tag{4}$$

where σ_{add} is the stress increase on a material element at a distance r from the crack tip. Motivated by the above result of fracture mechanics, the fiber bundle model can be

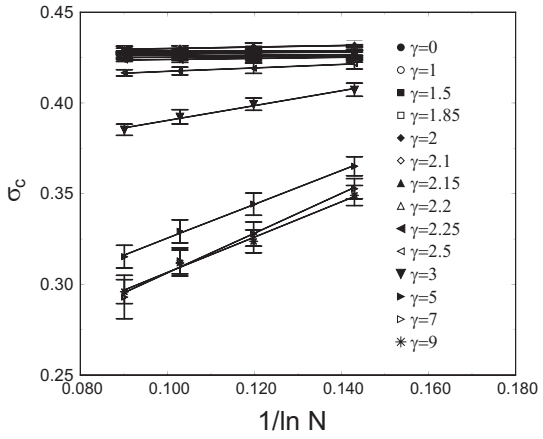

Figure 2: Variation of σ_c with the number of fibers of the bundle N at different γ values.

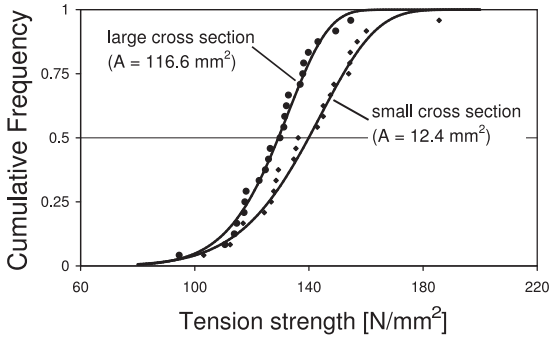

Figure 3: Strength cumulative distribution from wood specimens with different sizes.

amended by introducing a load sharing rule of the form of Eq. 4.

In the model the additional load received by an intact fiber i depends on its distance r_{ij} from a fiber j which has just been broken. Furthermore, elastic interaction is assumed between fibers such that the load received by a fiber follows a power law form. Hence, in the discrete model the stress-transfer function $F(r_{ij}, \gamma)$ takes the form

$$F(r_{ij}, \gamma) \propto r_{ij}^{-\gamma}, \tag{5}$$

where γ is an adjustable parameter and r_{ij} is the distance of fiber i to the rupture point (x_j, y_j). It can be seen that in the limits $\gamma \to 0$ and $\gamma \to \infty$ the load transfer function Eq. 5 recovers the two extreme cases of load redistribution of fiber bundle models, i.e. global and local load sharing, respectively.

3.2 Simulation Results

Computer simulations of the model described above with the fibers arranged on a two dimensional square lattice of size L and Weibull distributed strength values, Eq. 1 ($m = 2,\ \lambda = 1$), were performed varying the effective range of interaction γ over a broad interval. The avalanche size distribution, the cluster size distribution, and the ultimate strength of the bundle for several system sizes L were recorded. Each numerical simulation was repeated over at least 50 different realizations of the disorder distribution. Fig. 2 shows the ultimate strength σ_c of the fiber bundle for system sizes from $L = 33$ to $L = 257$ and different values of the parameter γ. Two distinct regimes can be clearly distinguished: for small γ, the strength σ_c is independent of the system size L. At a given point $\gamma = \gamma_c$ a crossover is observed, where γ_c falls in the vicinity of $\gamma = 2$. For large γ all curves decrease with $N \to \infty$ as

$$\sigma_c(N) \sim \frac{\alpha}{\ln N} \quad . \tag{6}$$

This qualifies for a genuine short range behavior as found in LLS models, where the same relation was obtained for the asymptotic strength of the bundle [4].

It is worth noting that a similar crossover at $\gamma \approx 2$ from GLS to LLS behavior is also present in the avalanche size distribution. Moreover, a detailed analysis of the distribution of cluster sizes, i.e. clusters of broken fibers preceding failure, confirms this crossover.

3.3 Size scaling of the strength of natural fiber composites

In [14], a combined experimental and theoretical study on the size dependence of tension strength of clear wood is presented, when loading is parallel to the fiber direction. The macroscopic strength of the tested softwood examples displays statistical variations, which can be fitted with a Weibull distribution, Eq. 1, with a shape parameter $\lambda \approx 8 \ldots 10$, see Fig. 3. The mean strength of the samples can be seen to exhibit a strong dependence on the sample size. The fracture behavior of the specimens is quite brittle and the variable range of interaction model is employed to assess the microscopic damage evolution. Here, a sample is represented by an array of parallel fibers arranged on a rectangular lattice, which is in accordance with the morphological structure of the material on the microscale. The empirical results can be fit with the model to obtain a numerical estimate of the load sharing parameter γ of Eq. 5, which yields $5 < \gamma < 10$, i.e. the load sharing is strongly localized.

4 Continuous Damage

In the following, we introduce a so-called continuous damage fiber bundle model (CDFBM) as an extension of the classical FBM by generalizing the damage law of fibers. We assume

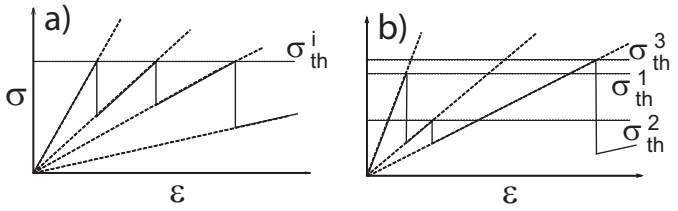

Figure 4: The damage law of a single fiber of the continuous damage model for quenched (a) and annealed (b) disorder, when multiple failure is allowed. The horizontal lines indicate the damage thresholds σ_{th}^i.

that the stiffness of fibers gradually decreases in consecutive failure events [15; 16].

The continuous damage model is composed of N parallel fibers with identical Young-modulus E and random failure thresholds σ_{th}^i. The fibers are assumed to have linear elastic behavior up to breaking (brittle failure), but at the failure point the stiffness of the fiber is reduced by a factor a, where $0 \leq a < 1$, i.e. the stiffness of the fiber after failure is aE. A fiber can now fail more than once and the maximum number k_{max} of failures allowed is a parameter of the model. Once a fiber has failed, its damage threshold σ_{th}^i can either be kept constant for the further breakings (quenched disorder, see Fig. 4a) or new failure thresholds of the same distribution can be chosen (annealed disorder, see Fig. 4b), which can model some microscopic rearrangement of the material after failure. The characterization of damage by a continuous parameter corresponds to describing the system on length scales larger than the typical crack size. This can be interpreted such that the smallest elements of the model are fibers and the continuous damage is due to cracking inside fibers. However, the model can also be considered as the discretization of the system on length scales larger than the size of single fibers, so that one element of the model consists of a collection of fibers with matrix material in between. In this case the microscopic damage mechanism resulting in multiple failure of the elements is the gradual cracking of matrix and the breaking of fibers. After failure the fiber skips a certain amount of load which has to be taken by the other fibers. For the load redistribution we assume infinite range of interaction among fibers (GLS); furthermore, an equal strain condition is imposed which implies that stiffer fibers of the system carry more load. At a strain ε, the load of a fiber i that has failed $k(i)$ times reads as

$$f_i(\varepsilon) = Ea^{k(i)}\varepsilon, \tag{7}$$

where $Ea^{k(i)}$ is the actual stiffness of fiber i. It is important to note that, in spite of the infinite interaction range, Eq. 7 is different from the usual global load sharing, where all the intact fibers always carry the same amount of load. In the following, the initial fiber stiffness E will be set to unity.

The constitutive behavior can be derived analytically. The variants of fiber bundle models which are widespread in the literature can be recovered by special choices of the parameters k_{max} and a of the model, such as a micromechanical model of composites [17; 18; 19; 20] or the classical FBM. The term of the highest failure index k_{max} can be conceived such that the fibers have a residual stiffness of $a^{k_{max}}$ after having failed k_{max} times. This residual stiffness results in a hardening of the material, hence, the $\sigma(\varepsilon)$ curves in Fig. 5a asymptotically tend to straight lines with a slope $a^{k_{max}}$. Increasing k_{max} the hardening part of the constitutive behavior is preceded by a longer and longer plastic plateau, and in the limiting case of $k_{max} \to \infty$ the materials behavior becomes completely plastic. A similar plateau and asymptotic linear hardening has been observed in brittle matrix composites.

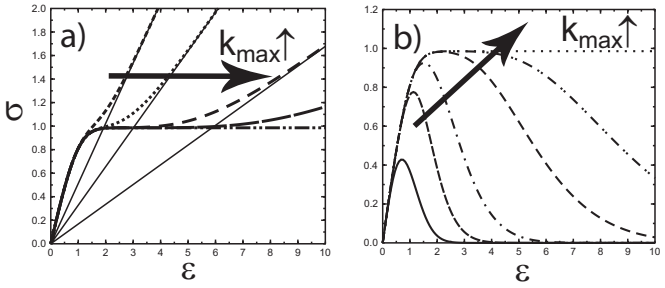

Figure 5: Constitutive behavior of the model of annealed disorder with residual stiffness (a) and quenched disorder without residual stiffness (b) at $a = 0.8$ for different values of k_{max}.

We can also account for macroscopic cracking and global failure of a specimen instead of hardening, by setting the residual stiffness of the fibers to zero after a maximum number k^* of allowed failures [16; 21]. A comparison of the constitutive laws of the dry and continuous damage FBM with global failure is presented in Fig. 5b. One can observe that the dry FBM constitutive law has a relatively sharp maximum, while the continuous damage FBM curves exhibit a plateau whose length increases with increasing k^*. Note that the maximum value of σ corresponds to the macroscopic strength of the material; furthermore, in stress controlled experiments the plateau and the decreasing part of the curves cannot be reached. However, by controlling the strain ε, the plateau and the decreasing regime can also be realized. The value of the driving stress σ corresponding to the plastic plateau, and the length of the plateau are determined by the damage parameter a, and by k_{max}, k^*: decreasing a at a fixed k_{max}, k^*, or increasing k_{max}, k^* at a fixed a gives rise to an increase of the plateau's length.

Computer simulations revealed that varying the two parameters of the model k_{max}, a, or k^*, a, and the type of dis-

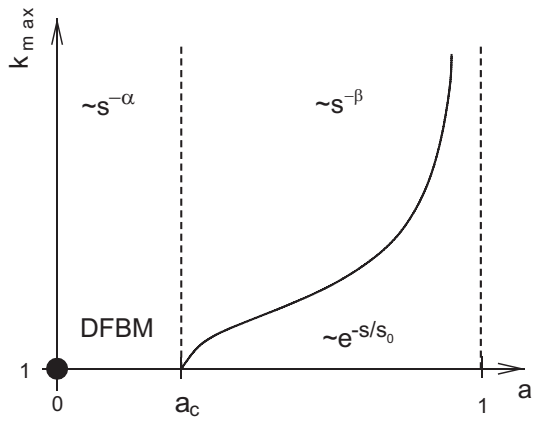

Figure 6: Phase diagram for the continuous damage model with remaining stiffness for both types of disorder. The functional form of the avalanche statistics is given in the parameter regimes. The location of DFBM in the parameter space is also indicated.

order, the CDFBM shows an interesting variety of avalanche activities, characterized by different shapes of the avalanche size distributions. On the basis of these simulation results, a phase diagram is constructed, see Fig. 6. If the damage parameter a is smaller than a_c, the dynamics of avalanches is close to the classical dry fiber bundle model (DFBM) characterized by a power law of the mean field exponent $\alpha = 5/2$. However, for $a > a_c$ the avalanche size distribution depends on the number of failures k_{max} allowed. The curve of $k_c(a)$ in the phase diagram separates two different regimes. For the parameter regime below the curve, avalanche distributions with an exponential shape were obtained. On the contrary, the parameter regime above $k_c(a)$ is characterized by a power law distribution of avalanches with a constant exponent $\beta = 2.12 \pm 0.05$, significantly different from the mean field exponent $\alpha = 5/2$ [10; 22; 23]. It is important to emphasize that the overall shape of the phase diagram is independent of the type of the disorder (annealed or quenched). Moreover, the specific values $a_c \approx 0.3$ and $k_c(a)$ depend on the details of the disorder distribution $p(\sigma_{th})$.

It is interesting to note that an "inverted" variant of this model has been applied successfully [24] to model force chains [25] in granular media under compression.

5 Beam Model

Solid blocks are often joined together by welding or glueing of the interfaces which are expected to sustain various types of external loads. Besides welded joints, glued interfaces of solids play a crucial role in fiber reinforced composites where fibers are embedded in a matrix material. Under shear loading of these interfaces complex deformation states of material elements can arise, leading to a complex degradation process [26], which cannot be captured by FBMs. We propose a novel approach to the shear failure of glued interfaces by extending the classical fiber bundle model to represent interfacial failure [27].

In our model the interface is discretized in terms of elastic beams which can be elongated and bent when exposed to shear load, see Fig. 7. The beams are assumed to have identical geometrical extensions (length l and width d) and linearly elastic behavior characterized by the Young modulus E. Failure of a beam can occur under two breaking modes, i.e. stretching and bending, which can be either independent or coupled by an empirical breaking criterion. Assuming that the two breaking modes are independent, a beam breaks if either the longitudinal stress t or the bending moment m exceeds the corresponding breaking threshold, see Fig. 7. Since the longitudinal stress t and the bending moment m acting on a beam can easily be expressed as functions of the longitudinal deformation ε, the breaking conditions can be formulated in a transparent way in terms of ε. To describe the relative importance of the breaking modes, we assign to each beam two breaking thresholds $\varepsilon_1^i, \varepsilon_2^i$, $i = 1, \ldots, N$, where N denotes the number of beams. The threshold values ε_1 and ε_2 are randomly distributed according to a joint probability density function $p(\varepsilon_1, \varepsilon_2)$ between lower and upper bounds $\varepsilon_1^{min}, \varepsilon_1^{max}$ and $\varepsilon_2^{min}, \varepsilon_2^{max}$, respectively. We can either for two independent breaking modes of a beam that are functions f and g of the longitudinal deformation ε. A single beam breaks if either its stretching or bending deformation exceeds the respective breaking threshold ε_1 or ε_2, i.e. failure occurs if

$$\frac{f(\varepsilon)}{\varepsilon_1} \geq 1, \quad \text{or} \tag{8}$$

$$\frac{g(\varepsilon)}{\varepsilon_2} \geq 1, \tag{9}$$

which will be called the OR breaking rule. Eqs. (8,9) describe the stretching and bending breaking modes, respectively. The failure functions $f(\varepsilon)$ and $g(\varepsilon)$ can be determined from the elasticity equations of beams, but in general the only restriction upon them is monotonicity in ε. In the specific case of sheared beams they take the form

$$f(\varepsilon) = \varepsilon\,, \quad g(\varepsilon) = a\sqrt{\varepsilon}, \tag{10}$$

where a is a constant and the value of the Young modulus E is set to 1. Assuming the thresholds of the two breaking modes to be independently distributed, the disorder distribution factorizes, $p(\varepsilon_1, \varepsilon_2) = p_1(\varepsilon_1)p_2(\varepsilon_2)$, and $\sigma(\varepsilon)$ takes the simple form

$$\sigma = \varepsilon[1 - P_1(f(\varepsilon))][1 - P_2(g(\varepsilon))]. \tag{11}$$

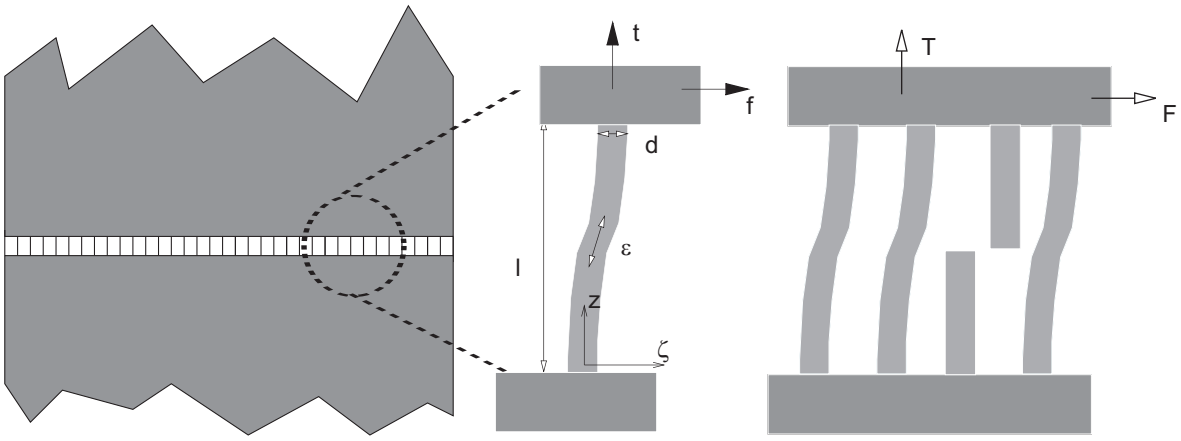

Figure 7: Illustration of the model construction. The sheared interface is discretized in terms of beams ($left$), which suffer stretching and bending deformation ($middle$) and fail due to the two deformation modes ($right$).

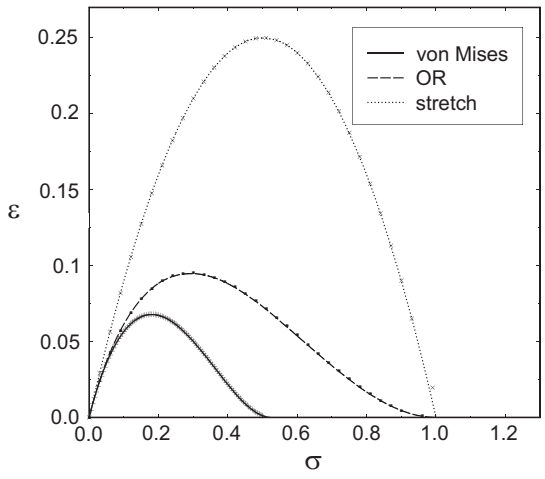

Figure 8: Constitutive curves of a simple dry fiber bundle ("stretch") and of the beam model with different breaking criteria.

The terms $1 - P_1(f(\varepsilon))$ and $1 - P_2(g(\varepsilon))$ provide the fraction of beams that failed under the stretching and bending breaking modes, respectively.

When the two breaking modes are coupled by a von Mises type breaking criterion, a single beam breaks if its strain ε fulfils the condition

$$\left(\frac{f(\varepsilon)}{\varepsilon_1}\right)^2 + \frac{g(\varepsilon)}{\varepsilon_2} \geq 1 \ . \tag{12}$$

Here, the constitutive curve in general cannot be obtained analytically. The constitutive curves obtained with the OR and von Mises breaking criteria are illustrated in Fig. 8 for the specific case of a uniform distribution between $\varepsilon_1^{min} = \varepsilon_2^{min} = 0$ and $\varepsilon_1^{max} = \varepsilon_2^{max} = 1$, *i.e.* $P_1(\varepsilon) = \varepsilon$ and $P_2(\varepsilon) = \varepsilon$.

It follows from the structure of Eq. 11, and it can be seen in Fig. 8, that the existence of two breaking modes leads to a reduction of the strength of the material, i. e. both the critical stress σ_c and strain ε_c take smaller values compared to the case of a single breaking mode applied in simple fiber bundle models [2; 9; 10; 12; 15]. The coupling of the two breaking modes by the von Mises form Eq. 12 gives rise to further reduction of the interface strength. We studied the effect of the disorder distribution of beams on the relative importance of the two breaking modes and on the progressive failure of the interface, considering independently distributed breaking thresholds with Weibull distributions of exponents m_1 and m_2, and scale parameters λ_1 and λ_2 for the stretching and bending modes, respectively.

It is interesting to note that varying the relative importance of the two failure modes gives also rise to a change of the macroscopic constitutive behavior of the system. Shifting the strength distributions of beams, the functional form of the constitutive behavior remains the same; however, the value of the critical stress and strain vary in a relatively

broad range. Varying the amount of disorder in the breaking thresholds, *i.e.* the Weibull exponents, has a similar strong effect on the macroscopic response of the system. Applying the von Mises breaking criterion, the microscopic and macroscopic response of the interface show similar behavior. The numerical analysis of the microscopic failure process of the interface revealed that the size of avalanches of simultaneously failing beams under a stress-controlled loading of the interface has a power law distribution, with the usual mean field exponent of 5/2. It has therefore been shown that the beam model for interfaces can be mapped onto a classical FBM by a suitable choice of the disorder distribution.

6 Plastic Model

During the gradual failure of interfaces of solid blocks under shear, damaged regions of the interface can still transmit load contributing to the overall load bearing capacity of the interface. This can occur, for instance, when the two solids remain in contact at the failed regions and exert friction force on each other. In many applications the glue between the two interfaces has disordered properties but its failure characteristics are not perfectly brittle. The glue under shear may also yield, carrying a constant load above the yield point.

We present an extension of fiber bundle models considering that failed fibers still carry a fraction $0 \leq \alpha \leq 1$ of their failure load. The value of α interpolates between the perfectly brittle failure ($\alpha = 0$) and the perfectly plastic behavior ($\alpha = 1$) of fibers [28].

6.0.1 Model construction and constitutive behavior

The disordered interface is represented by a parallel set of fibers with random breaking thresholds and linearly elastic behavior until failure. Since the equivalence of fiber and beam models—provided that an adequate failure threshold distribution is chosen—has been highlighted in the previous section, we restrict this discussion to an array of fibers.

Assuming global load sharing (GLS) after fiber breaking, the constitutive equation of the interface can be cast into a closed form. At an externally imposed deformation ε, the interface is a mixture of intact and broken fibers, which both contribute to the load bearing capacity of the interface. The constitutive equation $\sigma(\varepsilon)$ reads as

$$\sigma(\epsilon) = \underbrace{E\epsilon(1 - P(\epsilon)))}_{\sigma_{\mathrm{DFBM}}} + \underbrace{\alpha \int_0^{\epsilon} E\epsilon' p(\epsilon')\, d\epsilon'}_{\sigma_{\mathrm{Pl}}} \quad . \tag{13}$$

The first term, labeled σ_{DFBM}, provides the load carried by the intact fibers, which corresponds to the classical dry fiber bundle (DFBM) behavior. In the second term σ_{Pl}, which accounts for the load carried by the broken fibers, the integral is calculated over the entire load history of the interface up to the macroscopic deformation ε. It can be seen in Eq. 13 that the value of α controls the relative importance of the *elastic* and *plastic* terms, influencing both the macroscopic response $\sigma(\varepsilon)$ and the microscopic damage process of the system. When α is increased, less load is transferred to the intact fiber and in the limiting case $\alpha = 1$ failed fibers retain their entire load, so no load transfer occurs. In order to illustrate this behavior, Fig. 9 presents constitutive curves obtained by computer simulations of strain controlled loading, both for Weibull distributed fiber strength with $\lambda = 1$ and $m = 2$ and a uniform distribution. In the limiting case of $\alpha \to 1$ the constitutive curve $\sigma(\epsilon)$ reaches a plateau, indicating a perfectly plastic macroscopic state of the system.

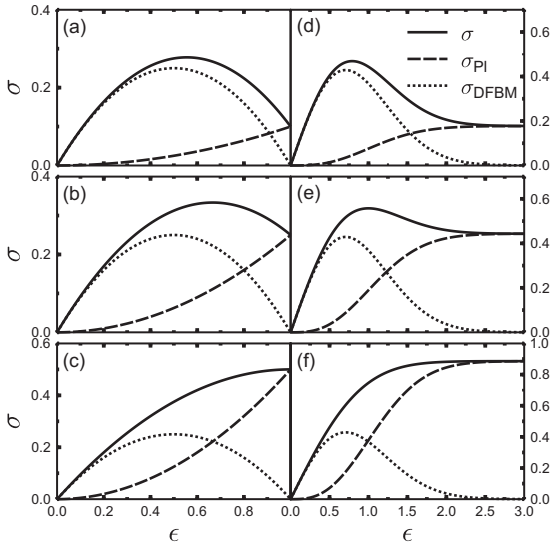

Figure 9: Constitutive behavior $\sigma(\epsilon)$ of the plastic fiber bundle for uniform (a, b, c) and Weibull distribution with $m = 2$ (d, e, f) at $\alpha = 0.2$ (a, d), $\alpha = 0.5$ (b, e) and $\alpha = 1.0$ (c, f). The contribution of intact σ_{DFBM} and of failed fibers σ_{Pl} are also shown.

6.0.2 Microscopic failure process

For GLS, avalanche size distributions $D(\Delta)$ obtained from computer simulations can be well fitted by a power law of exponent 5/2 for moderate values of α. However, for $\alpha > 0.9$ strong deviations from the power law can be observed, i. e. , the decay becomes much faster than in the classical FBM case.

The picture is somewhat different for localized load sharing. For $\alpha \approx 0$, due to the high stress concentration around failed fibers, the LLS bundle can only tolerate small

avalanches so that the avalanche size distribution $D(\Delta)$ decays rapidly. With increasing α, the higher amount of load kept by broken fibers can stabilize the bundle even after larger bursts, hence, the cut-off of the distributions moves to higher values. It is interesting to note that the functional form of the distribution $D(\Delta)$ also changes, i.e. when α approaches a critical value α_c the exponential cut-off disappears and the distribution becomes a power law

$$D(\Delta) \sim \Delta^{-\mu} \tag{14}$$

for large avalanches. The exponent μ was determined numerically as $\mu^{LLS} = 1.5 \pm 0.07$, which is significantly lower than the mean field value $\mu^{GLS} = 2.5$ [10] and corresponds to the value found for fiber bundles with critical disorder distributions [29; 30]. Increasing α above the critical point an exponential cut-off occurs and the power law regime of large avalanches gradually disappears. Above α_c the LLS distributions $D(\Delta)$ have the same functional form and follow the same tendency with increasing α as the GLS results.

In Fig. 10 the latest stable configuration of the bundle is presented just before catastrophic failure occurs at the critical load σ_c^{LLS} for several different values of α. For $\alpha \approx 0$ we note only small clusters of broken fibers as it is expected for LLS bundles (Fig. 10a). With increasing α, these clusters grow and adjacent clusters can even merge further increasing the typical cluster size (Fig. 10b). Around the critical value of $\alpha \approx 0.4$, a *spanning cluster* of broken fibers seems to appear (Fig. 10c), whereas for higher values of $\alpha > 0.4$ almost all fibers have failed (Fig. 10d) already by the time the critical stress is reached. The existence of very large clusters is the direct consequence of the increased load bearing capacity of broken fibers. In order to characterize the evolution of the cluster structure when α is changed and to reveal the nature of the transition at α_c, we calculated the average cluster size S_{av}. For each value of L, S_{av}has a maximum at a well-defined value of α, where the peak becomes higher and narrower for larger systems. The observed behavior is typical for continuous phase transitions, where the position of the maximum defines the critical point of the finite size system. In analogy to phase transitions, we performed a finite size scaling of S_{av} and other quantities and were able to determine the critical exponents. Contrary to global load sharing, this percolation-like transition has important physical consequences on the behavior of the fiber bundle. The failure process of the bundle is dominated by the competition of fiber breaking by local stress enhancement due to load redistribution, and by local weakness due to disorder. The relative importance of the two effects is controlled by the parameter α. Below the critical point $\alpha < \alpha_c$ the load carried by broken fibers has a stabilizing effect by limiting the stress concentration around cracks so that the failure of the bundle occurs due to localization. Above the critical

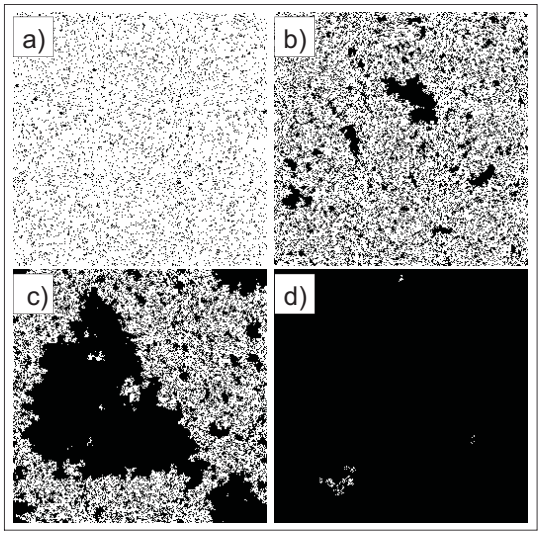

Figure 10: Latest stable configuration in LLS simulations of a system of size $L = 401$, with a Weibull strength distribution $m = 2$ at different values of the control parameter α (a) 0.0, (b) 0.35, (c) 0.4, (d) 0.6. Broken and intact fibers are indicated by black and white, respectively.

point $\alpha \geq \alpha_c$, the macroscopic response of the LLS bundle becomes practically identical with the GLS constitutive behavior, showing the dominance of disorder in this phase. On the macro-level, below the critical point $\alpha < \alpha_c$ the fiber bundle shows a brittle response, i.e. the macroscopic failure is preceded by a weak non-linearity, while for $\alpha \geq \alpha_c$ the constitutive behavior of the LLS bundle becomes practically identical with the GLS counterpart. The spanning cluster of failed fibers formed at the transition point proved to be compact with a fractal boundary whose dimension increases with the amount of disorder [28].

7 Conclusions

We presented an overview of recent extensions of the classical fiber bundle model in order to provide a more complete description of the fracture and breakdown of disordered materials. We gradually improved the model by generalizing the range of interaction of the fibers, damage law, deformation state, and the constitutive behavior. Analytical calculations and computer simulations were carried out to explore the macroscopic response and the microscopic damage process of the extended model, which was then confronted with the classical FBM intensively studied in the literature.

Recently, several applications of the extended fiber bundle models have been proposed in a broad range of breakdown phenomena. The continuous damage fiber bundle model with the gradual degradation of fiber strength proved to adequately describe the relevant damage mechanism of var-

ious types of materials. CDFBM was successfully applied to understand the strength and fracture mechanism of nacre [31; 32], where even a quantitative comparison to experimental findings was possible.

A viscoelastic FBM has been devised in [33; 34; 35], where a time-dependent formulation allows to describe creep rupture of fiber bundles. An interesting study of the viscoelastic fiber bundle model was performed in Refs. [36; 37], where the model was further improved considering a more realistic time dependent response of single fibers instead of Kelvin-Voigt elements [36]. The authors carried out creep rupture experiments on fiber composites with randomly oriented short fibers and found a quantitative agreement of the model predictions and experimental results on the macro- and micro-behavior of the system [37]. The careful analysis of the accumulation of damage in the viscoelastic fiber bundle model also helps to construct forecasting methods of the imminent macroscopic failure [38].

Considering the variable range model, short range interaction of fibers proved to be important for the mechanical behavior and rupture of biological tissues [39].

It has recently been shown that for GLS [29] as well as variable range respectively LLS cases [30] that fiber bundles with a lower cutoff in the disorder distribution show a crossover of the avalanche size distribution to an exponent $3/2$. The same situation is encountered when the recording of the avalanches starts close to the point of failure, which may have important consequences for the technical detection of imminent failure.

Based on a paper presented at CDCM06, the Conference on Damage in Composite Materials: Simulation and Non-Destructive Testing, Stuttgart, Germany, September 18./19. 2006.

F. Raischel and H.J. Herrmann are with ICP, University of Stuttgart, Pfaffenwaldring 27, D-70569 Stuttgart, Germany. H.J. Herrmann is also affiliated with IfB, ETH, Schafmattstr. 6, CH-8093 Zürich, Switzerland.

F. Kun is with the Department of Theoretical Physics, University of Debrecen, P.O. Box:5, H-4010 Debrecen, Hungary.

This work was supported by the Collaborative Research Center SFB 381. F. Kun acknowledges financial support of the Research Contracts NKFP 3A-043/2004, OTKA M041537, and T049209 and of the György Békésy Foundation of the Hungarian Academy of Sciences.

E-mail: raischel@icp.uni-stuttgart.de

References

[1] F. T. Peires: Tensile Tests for Cotton Yarns. v.-'the weakest link', Theorems on the Strength of Long Composite Specimens, in J. Textile Inst. **17** (1926), T355-368.

[2] H. E. Daniels: The Statistical Theory of the Strength of Bundles of Threads. I, in Proc. R. Soc London A **183** (1945), p. 405-435.

[3] B. D. Coleman: Time Dependence of Mechanical Breakdown Phenomena, in J. Appl. Phys. **27** (1956), p. 862.

[4] S. L. Phoenix and I. J. Beyerlein: Statistical Strength Theory for Fibrous Composite Materials, in A. Kelly C. Zweben, (Eds.): Comprehensive Composite Materials, volume 1, chapter 1.19, Pergamon-Elsevier Science (2000), p. 1-81.

[5] H. J. Herrmann and S. Roux (Eds.): Statistical Models for the Fracture of Disordered Media: Random Materials and Processes, Elsevier (1990).

[6] B. K. Chakrabarti and L. G. Benguigui: Statistical Physics of Fracture and Breakdown in Disordered Systems, Oxford University Press (1997).

[7] R. da Silveira: An Introduction to Breakdown Phenomena in Disordered Systems, in Am. J. Phys. **67** (1999), p. 1177.

[8] M. J. Alava and P. K. V. V. Nukala and S. Zapperi: Statistical models of fracture, in Adv. Phys. **55** (2006), p. 349.

[9] D. Sornette: Elasticity and Failure of a Set of Elements Loaded in Parallel, in J. Phys. A **22** (1989), L243-L250.

[10] M. Kloster, A. Hansen and P. C. Hemmer: Burst Avalanches in Solvable Models of Fibrous Materials, in Phys. Rev. E **56** (1997), p. 2615-2625.

[11] A. Hansen and P. C. Hemmer: Burst Avalanches in Bundles of Fibers: Local Versus Global Load-Sharing, in Phys. Lett. A **184** (1994), p. 394-396.

[12] R. C. Hidalgo, Y. Moreno, F. Kun and H. J. Herrmann: Fracture Model with Variable Range of Interaction, in Phys. Rev. E **65** (2002), p. 046148.

[13] W. I. Newman and A. M. Gabrielov: Failure of hierarchical distributions of fibre bundles. in Int. J. Fracture, **50**(1991), p. 1-14.

[14] G. Dill-Langer, R. C. Hidalgo, F. Kun, Y. Moreno, S. Aicher and H. J. Herrmann: Size Dependency of Tension Strength in Natural Fiber Composites, in Physica A **325** (2003), p. 547-560.

[15] R. C. Hidalgo, F. Kun and H. J. Herrmann: Bursts in a Fiber Bundle Model with Continuous Damage, in Phys. Rev. E **64** (6/2001), p. 066122.

[16] F. Kun, S. Zapperi and H. J. Herrmann: Damage in Fiber Bundle Models, in Eur. Phys. J. B **17** (2000), p. 269.

[17] F. Kun and H. J. Herrmann: Damage Development under Gradual Loading of Composites, in J. Mat. Sci. **35** (2000), p. 4685.

[18] S. L. Phoenix, M. Ibnabdeljalil and C.-Y. Hui: Size effects in the distribution for strength of brittle matrix fibrous composites, in Int. J. Solids Struct. **34** (1997), p. 545.

[19] S. L. Phoenix and R. Raj: Scalings in Fracture Probabilities for a Brittle Matrix Fiber Composite, in Acta metall. mater. **40** (1992), p. 2813.

[20] W. A. Curtin: The "Tough" to Brittle Transition in Brittle Matrix Composites, in J. Mech. Phys. Solids **41** (1993), p. 217.

[21] S. Zapperi, A. Vespignani and H. E. Stanley: Plasticity and Avalanche Behaviour in Microfracturing Phenomena, in Nature **388** (1997), p. 658.

[22] P. C. Hemmer and A. Hansen: The Distribution of Simultaneous Fiber Failures in Fiber Bundles, in J. Appl. Mech. **59** (1992), p. 909-914.

[23] S. Pradhan, A. Hansen and P. C. Hemmer: Crossover Behavior in Burst Avalanches: Signature of Imminent failure, in Phys. Rev. Lett. **95** (2005), p. 125501.

[24] R. C. Hidalgo, C. U. Grosse, F. Kun, H. W. Reinhardt and H. J. Herrmann: Evolution of Percolating Force Chains in Compressed Granular Media, in Phys. Rev. Lett. **89** (2002), p. 205501.

[25] C. Liu, S. R. Nagel, D. A Schecter, S. N. Coppersmith, S. Majumdar, O. Narayan and J. P. Witten: Force Fluctuations in Bead Packs, in Science **269** (1995), p. 513.

[26] S. Roux, A. Delaplace and G. Pijaudier-Cabot: Damage at Heterogeneous Interfaces, in Physica A **270** (1999), p. 35-41.

[27] F. Raischel, F. Kun and H. J. Herrmann: Simple Beam Model for the Shear Failure of Interfaces, in Phys. Rev. E **72** (2005), p. 046126.

[28] F. Raischel, F. Kun and H. J. Herrmann: Failure Process of a Bundle of Plastic Fibers, in Phys. Rev. E **73** (2006), p. 066101.

[29] S. Pradhan and A. Hansen: Failure Properties of Loaded Fiber Bundles Having a Lower Cutoff in Fiber Threshold Distribution, in Phys. Rev. E **72** (2005), p. 026111.

[30] F. Raischel, F. Kun and H. J. Herrmann: Local load sharing fiber bundles with a lower cutoff of strength disorder, in Phys. Rev. E **74** (2006), p. 035104(R).

[31] P. K. Nukala and S. Simunovic: Statistical Physics Models for Nacre Fracture Simulation, in Phys. Rev. E **72** (2005), p. 041919.

[32] P. K. Nukala and S. Simunovic: A Continuous Damage Random Thresholds Model for Simulating the Fracture Behavior of Nacre, in Biomaterials **26** (2005), p. 6087.

[33] R. C. Hidalgo, F. Kun and H. J. Herrmann: Creep Rupture of Viscoelastic Fiber Bundles, in Phys. Rev. E **65** (2002), p. 032502.

[34] F. Kun, R. C. Hidalgo, H. J. Herrmann and K. F. Pal: Scaling Laws of Creep Rupture of Fiber Bundles, in Phys. Rev. E **67** (6/2003), p. 061802.

[35] F. Kun, Y. Moreno, R. C. Hidalgo and H. J. Herrmann: Creep Rupture has Two Universality Classes, in Europhys. Lett. **63** (3/2003), p. 347-353.

[36] H. Nechad, A. Helmstetter, R. E. Guerjouma and D. Sornette: Creep Ruptures in Heterogeneous Materials, in Phys. Rev. Lett. **94** (2005), p. 045501.

[37] H. Nechad, A. Helmstetter, R. E. Guerjouma and D. Sornette: Andrade and Critical Time to Failure Laws in Fiber-Matrix Composites: Experiments and Model, in J. Mech. Phys. Solids **53** (2005), p. 1099.

[38] D. Sornette: Statistical Physics of Rupture in Heterogeneous Media, in S. Yip (Ed.): Handbook of Materials Modeling, Chapter 4.4. Springer Science and Business Media (2005).

[39] B. G. Yoon, J. Choi, M. Y. Choi: Connectedness and strength of biological organisms, in Journal of the Korean Physical Society **47** (2005), p. 1053